THE JOURNAL OF PHYSICAL CHEMISTRY A

Article

pubs.acs.org/JPCA

Effect of the Hydrogen Bond on Photochemical Synthesis of Silver Nanoparticles

Feng-jiao Zhao,[†] Lei Liu,[†,§] Yang Yang,[†,‡] Rui-ling Zhang,[†] Guang-hua Ren,[†] Da-li Xu,[†] Pan-wang Zhou,[†] and Ke-li Han*[,†]

[†]State Key Laboratory of Molecular Reaction Dynamics and [‡]Key Laboratory of Chemical Lasers, Dalian Institute of Chemical Physics, Chinese Academy of Sciences, Dalian 116023, China

[§]State Key Laboratory of Fine Chemicals, Dalian University of Technology, Dalian 116024, China

Supporting Information

ABSTRACT: The effect of a hydrogen bond on the photochemical synthesis of silver nanoparticles has been investigated via experimental and theoretical methods. In a benzophenone system, the photochemical synthesis process includes two steps, which are that hydrogen abstraction reaction and the following reduction reaction. We found that for the first step, an intermolecular hydrogen bond enhances the proton transfer. The efficiency of hydrogen abstraction increases with the hydrogen bond strength. For the second step, the hydrogen-bonded ketyl radical complex shows higher reducibility than the ketyl radical. The inductively coupled plasma-optical emission spectroscopy (ICP-OES) measurement exhibits a 2.49 times higher yield of silver nanoparticles in the hydrogen bond ketyl radical complex system than that for the ketyl radical system. Theoretical calculations show that the hydrogen bond accelerates electron transfer from the ketyl radical to the silver ion by raising the SOMO energy of the ketyl radical; thus, the SOMO−LUMO interaction is more favorable.

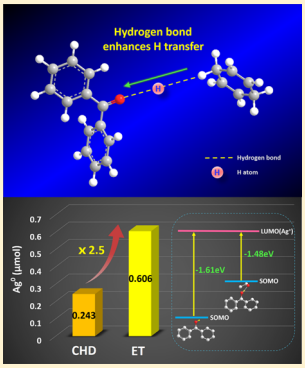

INTRODUCTION

The hydrogen bond (HB) widely exists in nature and has attracted extensive attention for its great importance in many science branches.[1−7] The HB plays vital roles in photophysical processes and photochemical reactions. Our group has reported a series of works that showed that the HB has an impact on photophysical and photochemical characteristics like absorption and fluorescence spectral red or blue shifts,[8] internal conversion (IC),[9] intersystem crossing (ISC),[8,10] intramolecular charge transfer (ICT),[11] photoinduced electron transfer,[12,13] excited-state proton transfer,[14] and so forth.[15−18] Moreover, the effect of an excited-state HB can be greatly strengthened or weakened depending on the photoexcitation of the hydrogen-bonded complexes.[19,20] For the ketone system, with the presence of the oxygen atom of carbonyl, the influence of the HB cannot be ignored. Particularly, when H donors have functional groups like hydroxyl (−OH), amino (>NH), and so on, the HB interaction in these systems will be more complicated.

As the most typical carbonyl compound photosensitizer, benzophenone (BP) is of intensive interest due to its extremely high efficiency of ISC ($\Phi_{ISC} \approx 1$) from the n → π^* singlet to the triplet.[21−23] The photophysical properties of BP have been studied and established: (1) BP absorbs UV light mostly at approximately 350 nm, (2) almost all of the BP S_1 goes to the lowest triplet state $T_1(n,\pi^*)$, which is highly reactive within 10 ps[23] through ISC and IC (Figure 1); (3) when suitable H donors exist, a hydrogen abstraction reaction occurs readily with the yielding of ketyl radicals.[21,22] The ketyl radical is well-known for strong reducibility. Thus, the ketyl radical is widely

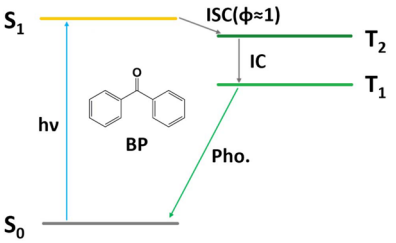

Figure 1. Electronic energy level of BP.

used in the synthesis of metal nanoparticles such as Ag, Au, Cu, and so forth as an electron donor. In this kind of photochemical synthesis, two main procedures are included: the hydrogen abstraction reaction, which produces ketyl radicals, and the reduction reaction, which yields metal nanoparticles. It is well accepted that a HB is always involved in the proton and electron transfers that are the key parts in the hydrogen abstraction reaction. The previous works show that the HB can enhance or prevent electron transfer, which is the common first step in the hydrogen abstraction reaction of amine based on different situations. For instance, Nishino et al. recently reported that at short-range, the HB conducts electrons better

Special Issue: Dynamics of Molecular Collisions XXV: Fifty Years of Chemical Reaction Dynamics

Received: October 11, 2015
Revised: November 12, 2015
Published: November 12, 2015

DOI: 10.1021/acs.jpca.5b09949
J. Phys. Chem. A 2015, 119, 12579−12585

than a covalent σ bond.[24] Moreover, Ishikita et al. found that the HB provides a highly efficient pathway of proton transfer.[25] These works demonstrate that the HB counts for much in electron transfer and proton transfer. Therefore, the effect of the HB on the photochemical synthesis of silver nanoparticles in the BP system is worth studying, and the dynamical study will help with revealing the reaction mechanism step by step and provide some guidance to optimize the photochemical reactions.

In this work, we carried out experiments and theoretical calculations to investigate the specific role of the HB on the photochemical synthesis of Ag nanoparticles in the BP system. Ethanol (ET) and 1,4-cyclohexadiene (CHD) are chosen as two types of H donors; ET and BP can form a ketyl radical complex linked by a HB after that hydrogen abstraction reaction, while CHD and BP will yield alone the ketyl radical because CHD has no atom of strong electronegativity like oxygen, nitrogen, and fluorine. The transient absorbance spectra and scan of total energy are performed to figure out the mechanism of the hydrogen abstraction reaction. Furthermore, in order to compare the synthesis efficiency of silver nanoparticles and the reduction capacity of two kinds of ketyl radicals, DFT calculations of the total energy scan, molecular orbital (MO) energy levels, and ionization energy (IE) have been conducted to give more information revealing the ketyl radical reduction mechanism. Experimentally, UV/vis absorption spectra of the Ag^0 plasmon band and inductively coupled plasma-optical emission spectroscopy (ICP-OES) measurements have been carried out to provide qualitative and quantitative comparisons.

EXPERIMENTAL AND THEORETICAL METHODS

General. BP and CHD were purchased from Alfa Aesar; silver nitrate ($AgNO_3$), ET, and the solvent acetonitrile (ACN) were obtained from Kermel. All of the chemicals were used as received without further purification. All experiments were conducted at room temperature (25 °C).

Laser Flash Photolysis (LFP). The transient absorbance spectra of BP with and without H donors were recorded by LFP. The wavelength of the nanosecond laser for excitation was 355 nm, and the laser energy was 25 mJ/pulse. The threshold of laser energy for excitation was measured and is shown in Figure S1. Samples (4 mL) were prepared in a quartz cell with a 10 mm optical path. A stock solution was prepared containing BP at the concentration of 5 mM. Sample solutions of BP (5 mM) were deaerated under nitrogen bubbling flow for 20 min. After that, H donors were immediately added into the samples using a microsyringe of desired concentration (50 mM), which guaranteed that the H donors were sufficient toward BP. Then, the samples were sealed with parafilm. The lifetimes of the BP triplets and ketyl radicals were analyzed by an exponential fitting method, and the results are shown in Figure S2.

Silver Plasmon Band (UV/Vis) Absorbance. Ag^0 plasmon band absorbance spectra were obtained using a PerkinElmer Lambda 35 UV/vis spectrometer immediately after irradiation. The laser settings were the same as those mentioned above. The stock solution was prepared of BP (1 mM) and $AgNO_3$ (1 mM) shortly before experiments. The following steps of deoxygenization and H donor (10 mM) injection were the same as those in LFP experiments. For the Ag^0 plasmon band absorbance spectra without BP, the stock solution was prepared of $AgNO_3$ (1 mM), and the laser set was the same as that in LFP experiments.

Inductively Coupled Plasma-Optical Emission Spectroscopy (ICP-OES). ICP-OES measurements of Ag^+ concentrations were performed to quantitatively characterize the synthesis efficiency. The stock solution was prepared of BP (1 mM) and $AgNO_3$ (1 mM). The following steps of deoxygenization and H donor (10 mM) injection were the same as those in LFP experiments. Because the sample solutions after UV irradiation contained both Ag^+ and Ag^0, the ICP-OES could not distinguish Ag^+ and Ag^0 but could distinguish the element Ag. Therefore, we tried to separate Ag^0 nanoparticles from Ag^+ in solution. Eventually, we adopted centrifugation to achieve this aim, and the validation of centrifugation is shown in Figure S3. The sample solutions after the desired-time UV irradiation were centrifuged for 40 min with a revolution speed of 15000 r/min. The upper liquid was used for ICP-OES measurements for $Ag^+_{\text{after irradiation}}$. Then, the amount of Ag^0 was deduced by

$$Ag^+_{\text{before irradiation}} - Ag^+_{\text{after irradiation}} = Ag^0_{\text{product}} \quad (1)$$

Theoretical Method. In this work, all theoretical calculations were accomplished using density functional theory (DFT) and time-dependent density functional theory (TDDFT) methods by Gaussian 09 programs.[26] In all DFT and TDDFT calculations, Becke's three-parameter hybrid exchange functional with Lee−Yang−Parr gradient-corrected correlation (B3LYP) was used. A basis set of 6-311++G(d,p) was chosen for C/H/O in the total energy scan of the radical reaction with Ag^+. The basis set in all other calculations was 6-31+G(d,p). For Ag^+, LANL2DZ was used due to it being a proper basis set for an ionic compound. For accuracy of the calculation in our systems, solvent correction was also considered, and the conductor-like polarizable continuum model (CPCM) was applied. In the calculation of the HB energy, the final results have been corrected by BSSE.

RESULTS AND DISCUSSION

First, we conducted the transient absorbance measurements, and the results are shown in Figure 2. Figure 2a displays the spectrum of BP without H donors; absorbance signals appeared from 500 to 610 nm, among which the strongest two peaks were at 530 and 600 nm. As shown in Scheme 1a, with the absence of H donors, all of these absorbance signals were attributed to triplet−triplet absorbance of BP $T_1(n,\pi^*)$. Our transient absorbance spectrum of BP T_1 agrees well with those in early works.[27−31]

When H donors existed, both excitation of BP and the hydrogen abstraction process occurred, resulting in the formation of a ketyl radical (Scheme 1b and c). For the BP−ET system, as shown in Scheme 1b, the ketyl radical product was a hydrogen-bonded complex. The corresponding spectrum was measured and is shown in Figure 2b. It is clear that the range of absorbance wavelengths is smaller, and this change is due to the quenching of BP T_1 by ET, which decreases the amount of BP T_1. In addition, although ET existed in solution, the absorbance at around 600 nm, which is the characteristic absorption peak of BP T_1,[27] still emerged, which meant that BP T_1 had not been completely quenched by ET and still could be observed. Thus, hydrogen abstraction of BP T_1 from ET is not that effective. In contrast, in the system of BP−CHD (Figure 2c), the strong absorbance peak only arose at 545 nm, and the absorbance peak at 600 nm completely disappeared. As for the BP ketyl radical and cyclohexadienyl, it is widely accepted that

DOI: 10.1021/acs.jpca.5b09949
J. Phys. Chem. A 2015, 119, 12579−12585

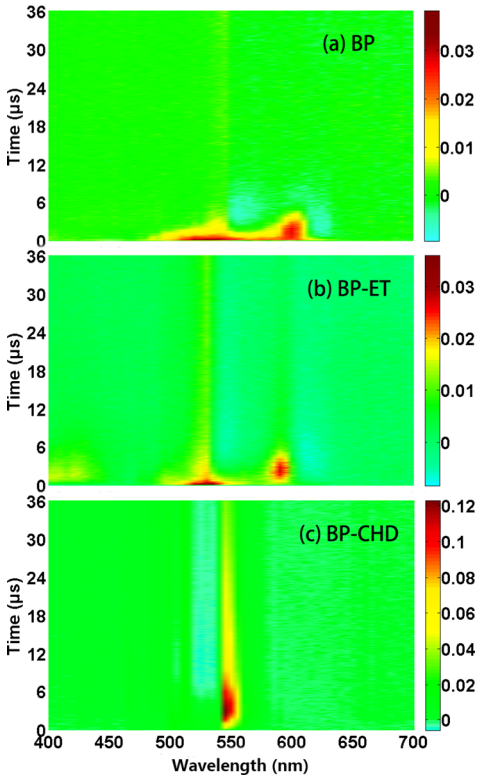

Figure 2. Transient absorbance (au) of BP (5 mM) with and without H donors (50 mM) in deaerated ACN. (a) BP; (b) BP with ET; (c) BP with CHD.

Scheme 1. (a) Excitation of BP and Hydrogen Abstraction Reactions of BP with (b) ET and (c) CHD

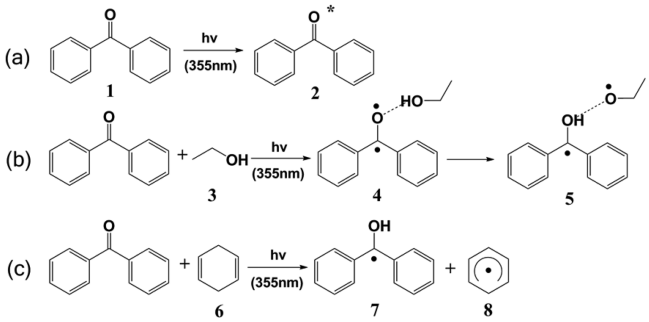

their characteristic absorbance peak is at around 530−550 nm. This indicates that BP T_1 had been thoroughly quenched within an ultrashort time. The overall transient spectra suggest that the hydrogen abstraction of BP T_1 from ET is weaker than that from CHD.

To understand the pathway of the hydrogen abstraction reaction and the influence of HB in BP−ET and BP−CHD systems, a scan of the total energy along the hydrogen abstraction pathway was obtained by the DFT/TDDFT method. As shown in Figure 3, we scanned the total energy at an interval of 0.1 Å and took the lowest stable energy as zero in both systems. Figure 3a shows that when the distance between O (ketyl) and H (−OH of ET) is greater than 2.02 Å, the hydrogen abstraction reaction will not happen. When O (ketyl) and H (−OH of ET) get closer, a potential barrier of 9.10 kcal/mol has to be overcome to transfer the hydrogen atom toward BP T_1. Contrastingly, in the system of BP−CHD

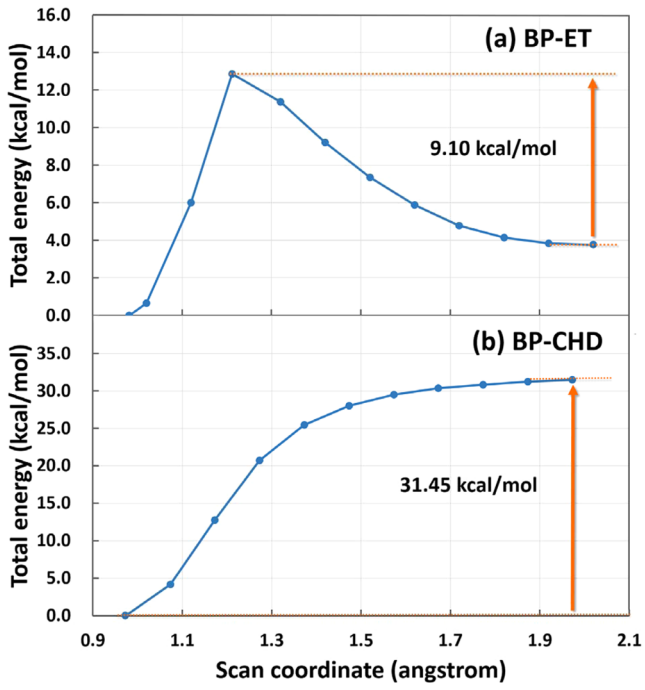

Figure 3. Theoretical calculation of scanning the total energy through the hydrogen abstraction process: (a) BP with ET; (b) BP with CHD.

(Figure 3b), the hydrogen abstraction process of BP T_1 from CHD is a barrier-free reaction. It means that once O (ketyl) and H (−CH_2 of CHD) are at a distance less than 2 Å, the hydrogen abstraction will readily and rapidly occur without any obstruction. Moreover, the final total energy of the ketyl radical and cyclohexadienyl radical is 31.45 kcal/mol lower than that of BP T_1 and CHD. This high-energy loss will make the products much more stable, and the hydrogen abstraction reaction in the BP−CHD system will be highly favorable. This theoretical result is consistent with the transient absorbance spectra result.

In addition, as displayed in Figure 4, the HBs in BP−ET and BP-CHD systems are different. Before the hydrogen abstraction

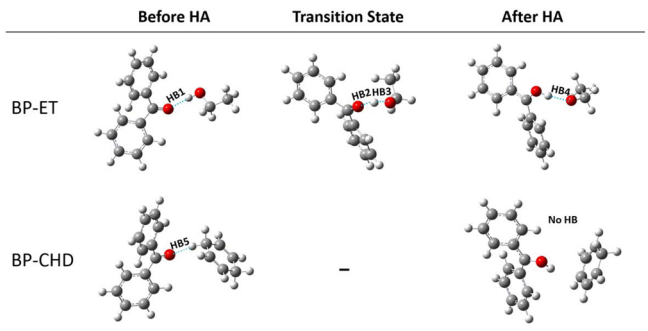

Figure 4. Views of the optimized structures for BP−ET and BP−CHD during the hydrogen abstraction (HA) reaction using B3LYP. Gray: C; white: H; red: O; blue: HB. Note: "–" means there are no such structures.

reaction, both systems have HBs, which are HB1 and HB5. For the transient state in the BP−ET system, HB2 and HB3 coexist. As for the stable structures after the hydrogen abstraction reaction, the HB exists only in the BP−ET system, which is HB4. The correlative information on these HBs was obtained using the DFT/B3LYP method and is listed in Table 1. It

DOI: 10.1021/acs.jpca.5b09949
J. Phys. Chem. A 2015, 119, 12579−12585

Table 1. HB Length, Dihedral Angle, and Energy in BP−ET and BP−CHD Systems during the Hydrogen Abstraction Reaction

	bond length (Å)	bond (dihedral) angle (deg)	bond energy (kJ/mol)
HB1	1.876	174.28	18.81
HB2	1.212	165.84	55.45
HB3	1.149	165.84	61.52
HB4	1.840	167.74	11.30
HB5	2.896	169.00	26.56

shows that before the hydrogen abstraction reaction, the bond lengths of HB1 and HB5 were 1.876 and 2.896 Å and the bond energies of HB1 and HB5 were 18.81 and 26.56 kJ/mol, respectively. The higher bond energy of HB5 indicates that the attraction of O (BP) for H from CHD is stronger than that from ET. Moreover, during the hydrogen abstraction in the BP−ET system, HB3 inhibits the hydrogen abstraction by offering the backward attraction force along the pathway of hydrogen transfer. These calculation results explain the transient absorbance spectra where hydrogen abstraction is more favorable in the BP−CHD system. In addition, Hibbert et al. have reported that for OHO HB systems, there will be potential barrier for proton transfer, and the weaker the HB, the higher the potential barrier.[32] Thus, the potential barrier of the hydrogen abstraction reaction in the BP−ET system shown in Figure 3a will be reasonable.

The ketyl radical, the product of the hydrogen abstraction reaction, is highly reactive and well-known to reduce metal ions such as Ag^+, Au^{3+}, Pd^+, Pt^+, and Au^{2+} with generating metal nanoparticles.[33−40] Ag nanoparticles have attracted wide attention because of unique and excellent performance in catalysis and biomedicine.[41] The mechanism of synthesis of Ag nanoparticles is shown in Scheme 2.

Scheme 2. Reduction of Silver Ions by the Ketyl Radical

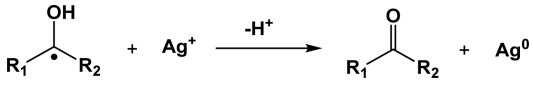

For Ag^0 synthesis efficiency, the ability of electron transfer from radicals to Ag^+ is the key factor. It is well-known that HB always plays vital roles in the electron-transfer process; therefore, the effect of the HB on Ag^0 synthesis will be worth studying. As mentioned above, the ketyl radicals produced in BP−ET and BP−CHD systems are different (shown in Scheme 1). Therefore, these two kinds of radicals will well-represent the effect of the HB on Ag^0 photosynthesis.

First, we performed the DFT calculations that scanned the total energy along the pathway of electron transfer. The results are shown in Figure 5. The horizontal axis represents the distance (Å) between C of ketyl and Ag^+, and the vertical axis is the total energy (kcal/mol). In the ketyl radical complex system (Figure 5a), the electron transfer occurs at a distance of 2.8 Å, and an energy of 3.77 kcal/mol is needed. In contrast, in the ketyl radical system (Figure 5b), this distance is 2.7 Å, which means that the ketyl radical and Ag^+ have to be 0.1 Å closer for electron transfer occur. Moreover, a higher energy of 4.58 kcal/mol is required in this reaction. As a result, the DFT calculations indicate that the electron-transfer reaction between the radical and Ag^+ will be more favorable in the ketyl radical complex system than that in the ketyl radical system.

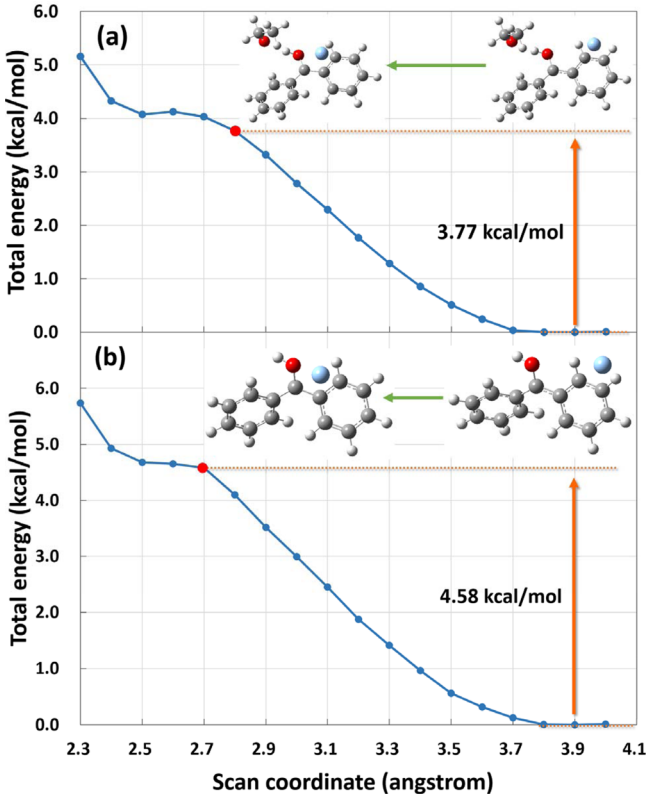

Figure 5. Theoretical calculation of scanning the total energy through the reaction pathway of electron transfer from radicals to Ag^+, at the level of DFT/B3LYP/6-311++G(d,p) for C/H/O; LANL2DZ for Ag. The radicals in two different systems are (a) the ketyl radical complex in the BP−ET system and (b) the ketyl radical in the BP−CHD system. The insets show configurations of the radical and Ag^+ before and after reaction. Gray: C; white: H; r: O; blue: Ag.

In order to compare the efficiency of Ag nanoparticle synthesis between BP−ET and BP−CHD systems, UV/vis absorbance spectra of the Ag^0 plasmon band experiment have been obtained, and the results are shown in Figure 6. It is well accepted that the Ag^0 plasmon band absorbance wavelength ranges from 350 to 600 nm, which depends on the size of nanoparticles.[42−46] Generally, the absorbance wavelength of Ag^0 nanoparticles in a size range of 10−100 nm is 400−420 nm. As shown in Figure 6, it is clear that the absorbance peak appears at 400 nm, and the intensity increases as the irradiation time gets longer. For irradiation times of 90 and 300 s, the maximum absorbance values of Ag^0 in the BP−ET system are 0.1241 and 0.219, respectively. In contrast, in the BP−CHD system, the maximum absorbance values at 400 nm for 90 and 300 s are 0.101 and 0.1128, respectively. It suggests that the amount of Ag^0 in the BP−ET system is more than that in the BP−CHD system after the same irradiation time. This result indicates that the ketyl radical complex would be a more efficient reductant than the ketyl radical. Considering that the absorbance wavelength involves the Ag^0 nanoparticle size, the absorbance peak at a wavelength of 400 nm stands only for the Ag^0 nanoparticles of 10−100 nm in size. Actually, the reduction efficiency should be characterized by the total Ag^0. Therefore, the UV/vis absorbance spectra provide merely a qualitative comparison of reduction efficiency.

For accurate and quantitative comparison, ICP-OES measurement was conducted, and the result is shown in Figure 7. In the ICP-OES experiment, the irradiation time was set to

DOI: 10.1021/acs.jpca.5b09949
J. Phys. Chem. A 2015, 119, 12579−12585

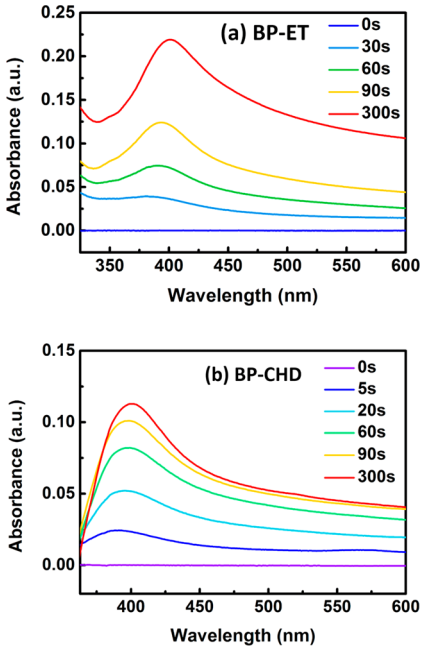

Figure 6. Ag^0 plasmon band UV/vis absorbance spectra for irradiation times of 0−300 s. (a) BP (1 mM), ET (10 mM), and $AgNO_3$ (1 mM); (b) BP (1 mM), CHD (10 mM), and $AgNO_3$ (1 mM).

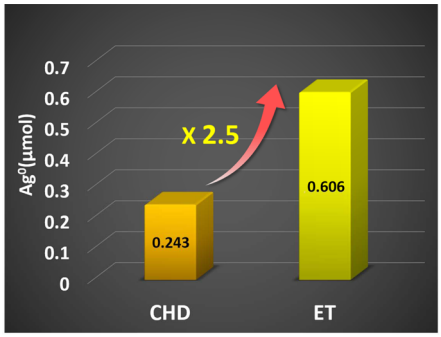

Figure 7. Yield of Ag^0 for an irradiation time of 20 s in the ketyl radical complex (BP−ET) system and the ketyl radical (BP−CHD) system.

20 s. This short time of irradiation is to make sure that the Ag^+ will be adequate after 20 s and prevent the inaccuracy that is caused by Ag^+ exhaustion. It shows that for the BP−ET system, 0.606 μmol of Ag^0 has been formed. As for the BP−CHD system, the amount of Ag^0 formed is 0.243 μmol. It is clear that the efficiency of synthesis of Ag nanoparticles in the BP−ET system is 2.49 times as much as that in the BP−CHD system. This difference of reduction reaction efficiency demonstrates that the ketyl radical complex has stronger reducibility than the ketyl radical for Ag nanoparticle synthesis.

In order to ensure that the Ag^+ consumption in the ICP-OES experiment is ascribed to ketyl radicals rather than the direct reduction of Ag^+ by ET and CHD, we carried out the UV/vis absorption spectra experiment of ET and CHD systems without BP to test the reducibility of ET and CHD under the conditions in this work. The results are shown in Figure 8. From the absorbance curves at 0 s in both ET and CHD systems, we can find no absorption at 355 nm, which means that no species in either system can be excited at 355 nm. As the irradiation time increases to 60 s, there is no absorbance signal of the Ag^0 plasmon band at around 400 nm. This shows

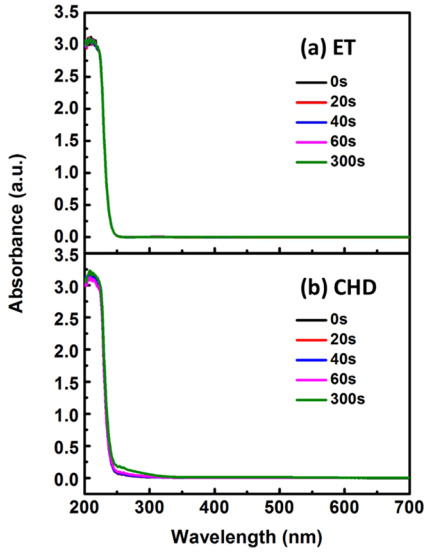

Figure 8. UV/vis absorbance spectra for different irradiation times in ET and CHD systems without BP: (a) ET (10 mM) and $AgNO_3$ (1 mM); (b) CHD (10 mM) and $AgNO_3$ (1 mM).

that no Ag^0 nanoparticle is produced in either system within 60 s. Considering that the reducibility of ET and CHD may be relatively weak in this condition and the Ag^0 plasmon band absorption would be "invisible" under irradiation of 60 s, we conducted a much longer irradiation time of 300 s. As shown in Figure 8, there is still no absorbance signal of the Ag^0 plasmon band at around 400 nm. This result demonstrates that ET and CHD cannot reduce Ag^+ to Ag^0 under 355 nm irradiation, and the Ag^+ consumption in the ICP-OES experiment comes from ketyl radicals.

To better understand the reason for the higher reducibility of the ketyl radical complex than the ketyl radical, we carried out the frontier MO calculations. Synthesis of Ag^0 from Ag^+ means an electron of another molecule fills the LUMO of Ag^+. Thus, when the energy level of the electron-donating MO is close to the LUMO of Ag^+, a reduction reaction will occur easily. For the ketyl radical, with the presence of a single electron, the electron-donating MO is the SOMO. The reduction reaction between the ketyl radical and Ag^+ is a SOMO−LUMO interaction. As displayed in Figure 9, the LUMO of Ag^+ is −2.89 eV, while the SOMOs of the ketyl radical complex and ketyl radical are −4.37 and −4.50 eV, respectively. It is obvious that the SOMO of the ketyl radical complex is closer to the LUMO of Ag^+. This smaller SOMO−LUMO energy gap is

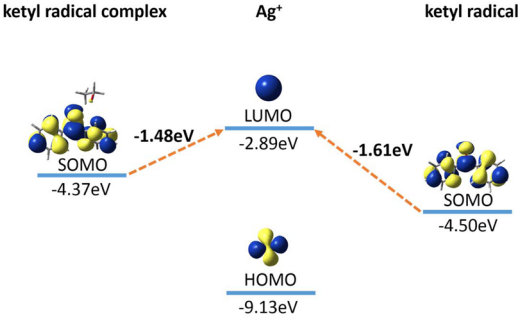

Figure 9. Calculated frontier MO HOMO and LUMO for Ag^+ and the SOMO for the ketyl radical complex and ketyl radical.

DOI: 10.1021/acs.jpca.5b09949
J. Phys. Chem. A 2015, 119, 12579−12585

more beneficial for an electron to transfer from the SOMO to LUMO.[47] As a result, the higher SOMO makes ketyl radical complex exhibit stronger reducibility than ketyl radical.

Furthermore, IE calculation has also been conducted to investigate the capacity of donating an electron. The IE of a radical is the energy that is required to remove an electron from the neutral radical to form a stable radical cation (eq 2).

$$\mathrm{IE} = E^{+}(\mathrm{opt}) - E^{0}(\mathrm{opt}) \quad (2)$$

Our calculation yielded an IE for the ketyl radical complex of 4.057 eV, while for the ketyl radical, it was 4.242 eV. The relatively smaller IE of the ketyl radical complex demonstrates that it is easier for the ketyl radical complex to lose an electron than the ketyl radical. The IE calculation result confirms that the hydrogen-bonded keytl radical complex is a better reductant than the keytl radical for Ag synthesis.

CONCLUSION

In summary, the intermolecular HB plays beneficial roles for the photochemical synthesis of Ag nanoparticles in the BP system. For the hydrogen abstraction reaction of BP and H donors, the intermolecular HB can accelerate the hydrogen transfer, and the efficiency of the hydrogen abstraction reaction is directly proportional to the HB strength. As for the following process of the reduction reaction, the hydrogen-bonded ketyl radical complex exhibits much higher reducibility than the ketyl radical for a higher yield of Ag nanoparticles. The higher SOMO energy level of the ketyl radical complex facilitates the SOMO−LUMO interaction.

ASSOCIATED CONTENT

Supporting Information

The Supporting Information is available free of charge on the ACS Publications website at DOI: 10.1021/acs.jpca.5b09949.

Laser energy threshold value measurement for the transient absorbance spectra, lifetimes of ketyl radicals, and centrifugation performance (PDF)

AUTHOR INFORMATION

Corresponding Author

*E-mail: klhan@dicp.ac.cn.

Notes

The authors declare no competing financial interest.

ACKNOWLEDGMENTS

This work is supported by the Natural Science Foundation of China (NSFC; Grant Nos. 21403226 and 21273234).

REFERENCES

(1) Lancaster, J. R.; Smilowitz, R.; Turro, N. J.; Koberstein, J. T. *Photochem. Photobiol.* **2014**, *90* (2), 394−401.
(2) Han, K.-L.; Zhao, G.-J. *Hydrogen Bonding and Transfer in the Excited State*; John Wiley & Sons: New York, 2011.
(3) Zhao, G.-J.; Liu, J.-Y.; Zhou, L.-C.; Han, K.-L. *J. Phys. Chem. B* **2007**, *111*, 8940−8945.
(4) Salamone, M.; Milan, M.; Dilabio, G. A.; Bietti, M. *J. Org. Chem.* **2013**, *78*, 5909−5917.
(5) Savéant J.-M. Tard C. *J. Am. Chem. Soc.*,201413689078910.
(6) Kiyota, T.; Yamaji, M.; Shizuka, H. *J. Phys. Chem.* **1996**, *100*, 672−679.
(7) Zhao, G.-J.; Han, K.-L. *J. Phys. Chem. A* **2009**, *113*, 14329−14335.
(8) Zhao, G. J.; Han, K. L. *Acc. Chem. Res.* **2012**, *45*, 404−413.
(9) Zhao, G. J.; Han, K. L. *J. Phys. Chem. A* **2007**, *111*, 9218−9223.
(10) Han, K. L.; He, G. Z. *J. Photochem. Photobiol., C* **2007**, *8*, 55−66.
(11) Zhao, G. J.; Han, K. L. *Biophys. J.* **2008**, *94*, 38−46.
(12) Yu, F.; Li, P.; Li, G.; Zhao, G.; Chu, T.; Han, K. *J. Am. Chem. Soc.* **2011**, *133*, 11030−11033.
(13) Zhao, G. J.; Liu, J. Y.; Zhou, L. C.; Han, K. L. *J. Phys. Chem. B* **2007**, *111*, 8940−8945.
(14) Zhao, G. J.; Han, K. L. *J. Chem. Phys.* **2007**, *127*, 024306.
(15) Zhao, G. J.; Northrop, B. H.; Han, K. L.; Stang, P. J. *J. Phys. Chem. A* **2010**, *114*, 9007−9013.
(16) Yang, D.; Yang, Y.; Liu, Y. *Commun. Comput. Chem.* **2013**, *1*, 205−215.
(17) Zhang, M.; Ren, B.; Wang, Y.; Zhao, C. *Commun. Comput.Chem.* **2013**, *1*, 216−224.
(18) Liu, Y.; Lan, S. *Commun. Comput. Chem.* **2013**, *1*, 235−243.
(19) Zhao, G. J.; Han, K. L. *J. Phys. Chem. A* **2007**, *111*, 2469−2474.
(20) Zhao, G. J.; Han, K. L. *ChemPhysChem* **2008**, *9*, 1842−1846.
(21) Griesbeck, A., Oelgemoller, M., Ghetti, F., Eds.; *CRC Handbook of Organic Photochemistry and Photobiology*, 3rd ed.; CRC Press: Boca Raton, FL, 2012.
(22) Hoshino, M.; Arai, S.; Imamura, M.; Ikehara, K.; Hama, Y. *J. Phys. Chem.* **1980**, *84*, 2576−2579.
(23) Turro, N. J.; Ramamurthy, V.; Scaiano, J. C. *Principles of molecular photochemistry: an introduction*; University Science Books: Sausalito, CA, 2010.
(24) Nishino, T.; Hayashi, N.; Bui, P. T. *J. Am. Chem. Soc.* **2013**, *135*, 4592−4595.
(25) Ishikita, H.; Saito, K. *J. R. Soc., Interface* **2014**, *11*, 20130518.
(26) Frisch, M. J.; Trucks, G. W.; Schlegel, H. B.; Scuseria, G. E.;Robb, M. A.; Cheeseman, J. R.; Scalmani, G.; Barone, V.; Mennucci, B.; Petersson, G. A.; et al. *Gaussian 09*; Gaussian, Inc.: Wallingford, CT, USA, 2010.
(27) Scaiano, J. C.; Abuin, E. B.; Stewart, L. C. *J. Am. Chem. Soc.* **1982**, *104*, 5673−5679.
(28) Bensasson, R. V.; Gramain, J.-C. *J. Chem. Soc., Faraday Trans. 1* **1980**, *76*, 1801−1810.
(29) Peters, K. S.; Freilich, S. C.; Schaeffer, C. G. *J. Am. Chem. Soc.* **1980**, *102*, 5701−5702.
(30) Cai, X.; Sakamoto, M.; Hara, M.; Sugimoto, A.; Tojo, S.; Kawai, K.; Endo, M.; Fujitsuka, M.; Majima, T. *Photochem. Photobiol. Sci.* **2003**, *2*, 1209−1214.
(31) Aloise, S.; Ruckebusch, C.; Blanchet, L.; Rehault, J.; Buntinx, G.; Huvenne, J.-P. *J. Phys. Chem. A* **2008**, *112*, 224−231.
(32) Hibbert, F.; Emsley, J. *Adv. Phys. Org. Chem.* **1991**, *26*, 255.
(33) Scaiano, J. C.; Aliaga, C.; Maguire, S.; Wang, D. *J. Phys. Chem. B* **2006**, *110*, 12856−12859.
(34) Scaiano, J. C.; Billone, P.; Gonzalez, C. M.; Marett, L.; Marin, M. L.; McGilvray, K. L.; Yuan, N. *Pure Appl. Chem.* **2009**, *81*, 635−647.
(35) Korchev, A. S.; Shulyak, T. S.; Slaten, B. L.; Gale, W. F.; Mills, G. *J. Phys. Chem. B* **2005**, *109*, 7733−7745.
(36) Korchev, A. S.; Konovalova, T.; Cammarata, V.; Kispert, L.; Slaten, L.; Mills, G. *Langmuir* **2006**, *22*, 375−384.
(37) Fouassier, J.-P.; Lalevée, J. *Photoinitiators for Polymer Synthesis: Scope, Reactivity and Efficiency*, 1st ed.; Wiley-VCH Verlag GmbH & Co. KGaA: Weinheim, Germany, 2012.
(38) Clary, D. R.; Nabil, M.; Sedeh, M. M.; El-Hasadi, Y.; Mills, G. *J. Phys. Chem. C* **2012**, *116*, 9243−9250.
(39) Yang, Y.; Lui, L.; Yin, H.; Xu, D.; Liu, G.; Song, X.; Liu, J. *J. Phys. Chem. C* **2013**, *117*, 11858−11865.
(40) Zielinska, A.; Skwarek, E.; Zaleska, A.; Gazda, M.; Hupka, J. *Procedia Chem.* **2009**, *1*, 1560−1566.
(41) Mayer, K. M.; Hafner, J. H. *Chem. Rev.* **2011**, *111*, 3828−3857.
(42) Kelly, K. L.; Coronado, E.; Zhao, L. L.; Schatz, G. C. *J. Phys. Chem. B* **2003**, *107*, 668−677.
(43) Mock, J. J.; Barbic, M.; Smith, D. R.; Schultz, D. A.; Schultz, S. *J. Chem. Phys.* **2002**, *116* (15), 6755.
(44) Pesika, N. S.; Stebe, K. J.; Searson, P. C. *J. Phys. Chem. B* **2003**, *107*, 10412−10415.

DOI: 10.1021/acs.jpca.5b09949
J. Phys. Chem. A 2015, 119, 12579−12585

(45) Saion, E.; Gharibshahi, E.; Naghavi, K. *Int. J. Mol. Sci.* **2013**, *14*, 7880−7896.
(46) Silvestrini, S.; Carofiglio, T.; Maggini, M. *Chem. Commun.* **2013**, *49*, 84−86.
(47) Maruani, J. *Molecules in Physics, Chemistry, and Biology 3, Electronic Structure and Chemical Reactivity*; Kluwer Academic Publishers: Norwell, MA, 1988.

DOI: 10.1021/acs.jpca.5b09949
J. Phys. Chem. A 2015, 119, 12579−12585